Effect of Ionic Strength on Surface-Selective Patch Binding-Induced Phase Separation and Coacervation in Similarly Charged Gelatin−Agar Molecular Systems

Shilpi Boral and H. B. Bohidar*

Polymer and Biophysics Laboratory, School of Physical Sciences, Jawaharlal Nehru University, New Delhi-110 067, India

Received: June 14, 2010; Revised Manuscript Received: August 12, 2010

Coacervate is defined as a polymer-rich dense phase, which remains in thermodynamic equilibrium with its low concentrated phase called the supernatant. The effect of ionic strength ($I = 0-0.1$ M NaCl) on the mechanism of surface patch binding-induced protein−polysaccharide interaction leading to complex coacervation, between agar (a polyanionic polysaccharide) and gelatin B (a polyampholyte protein), both having similar net charge, at a particular mixing ratio, [gelatin]/[agar] = 1, was studied at various temperatures (20−40 °C). The coacervation transition was probed by turbidity and zeta-potential measurements. The intermolecular association had the signature of surface-selective binding, and a model calculation could explain the potential energy of interactions operative in such processes. The thermo-mechanical features of the coacervates were found to be strongly dependent on ionic strength, which has been interpreted as originating from formation of salt-bridges between the biopolymers. The microstructure of the coacervate materials was analyzed using rheology and small angle neutron scattering (SANS) techniques, which probed the heterogeneity prevailing in the system that had characteristic length in the range 1.3−2.0 nm, and the same data yielded the correlation length of concentration fluctuations, which was estimated to lay in the range 2.4−4 nm. It is concluded that the coacervation transition driven by surface-selective binding is not influenced by the ionic strength of the solution, but the mobile ions participate in the structural organization of the interacting polyions in the coacervate.

1. Introduction

Protein−polysaccharide interactions have caught the attention of many scientists in recent past due to their inherent potential to generate new biomaterials. The formation of biopolymer−biopolymer supramolecular structures as coacervates induced by electrostatic interactions is a fundamental physiochemical phenomenon, relevant to a number of known biological processes such as protein transcription, antigen−antibody reactions, and enzymatic channeling. Recent literature[1] reveals that complex formation between weakly charged polyelectrolytes is driven by the negative enthalpy ΔH due to electrostatic attraction, with counterion release entropy playing only a minor role. On the other hand, the complex formation between highly charged polyelectrolyte is driven by large counterion release entropy and opposed by a positive enthalpy change. A large variation of counterion release entropy as a function of salt concentration was only detected for highly charged polyelectrolytes.[1] The molar heat capacity ΔC_p of the system plays a vital role in variation of binding enthalpy with the temperature. This originates from the changes in degree of surface hydration in the free and complex molecules. If ΔC_p has large positive values, the system leads to charge neutralization via the ionization process (protein−polysaccharide systems), if ΔC_p is negative, the system provokes hydrophobic interactions, and if ΔC_p is positive with negative ΔH at all temperatures, there is significant contribution of H-bonding.[1] In a recent study of the gelatin−agar system done in our laboratory,[2] no temperature effect was observed either on the critical pH of complex formation or on the pH where phase separation occurred. The phase separation was not promoted by electrostatic interactions, hydrogen bonding, or hydrophobic interactions but through polarization-induced attractive interactions. The main reason for such a complex formation was the existence of small "patches" on the protein, that is, localized regions with higher charge density. Here, the ion−dipole interaction overcomes ion−ion repulsion, or if the polyacid/polybase is strong enough or the protein has a high enough regulation capacity a reversal of charge may be induced on the protein.

Coacervation is a process during which a homogeneous solution of charged macromolecules undergoes liquid−liquid phase separation, giving rise to a polymer-rich dense phase called coacervates.[2−8] Coacervation has been classified into simple and complex processes depending on the number of participating macromolecules.[7] In simple polyelectrolyte coacervation, addition of salt or alcohol normally promotes coacervation. In complex coacervation, two oppositely charged macromolecules (or a polyelectrolyte and an oppositely charged colloid) can undergo coacervation through associative interactions. The charges on the polyelectrolytes must be sufficiently large to cause significant electrostatic interactions, but not so large to cause precipitation. The dilute liquid phase, usually the supernatant, remains in equilibrium with the coacervate phase. These two liquid phases are incompatible and immiscible.[7]

The formation of coacervates versus aggregates could be related to the stiffness and to the charge density of polysaccharides, more rigid ones leading to aggregates and flexible ones to coacervates. Agar is well-known for its rigid rod-shaped fiber bundles, which is stiff enough due to its high charge density,[3] whereas gelatin is known to bear a persistence length of 2 nm showing its flexible nature.[4] The phase separation could be

* Corresponding author. Tel.: +91 11 2674 4637. Fax: +91 11 2674 1837. E-mail: bohi0700@mail.jnu.ac.in.

10.1021/jp105431t
Published on Web 09/01/2010

visualized as a spinodal decomposition[5] or nucleation and growth[6] mechanism. However, it appears that all of the systems have their signature interaction mechanisms. For instance, the coacervation behavior of some polymers such as elastin[6] appears to be an example of mixed coacervation intermediate between the classes of unicomplex and simple coacervation as defined by Bungenberg de Jong.[7] Again, in some literature, we find that complex coacervates are highly unstable, and sometimes a toxic chemical agent such as gluteraldehyde is added to stabilize the material.[8] Several theoretical models have been proposed to address the phase separation kinetics that leads to coacervation transition. Some of these are Voorn−Overbeek,[9] Veis−Aranyi,[10] Nakajima− Sato,[11] Tainaka,[12] and Amarnath−Bohidar[13] models. The salient features of all of the models are discussed in ref 13. Coacervates are believed to have a weakly interconnected network system associated with strong concentration fluctuations that prevail over many length and time scales, which allows these systems to evolve dynamically with time.[14]

In a small class of systems, liquid−liquid phase separation gets initiated by surface-selective patch binding[15,16] even though both polyions carry a similar net charge. This is often referred to as binding on the wrong side of pH. In the present work, we have shown that the formation of intermolecular soluble complexes and the phenomenon of coacervation could be achieved when a polyelectrolyte (agar) interacts with a polyampholyte (gelatin) through surface-selective patch binding. Little is known about the effect of ionic strength on such binding mechanisms, which is the main focus of this work. To get a better feeling of the system, the results are compared to the salient features reported in gelatin simple coacervates,[17] and gelatin A−gelatin B,[18] gelatin−chitosan,[15] and gelatin A−agar[19] complex coacervates. The surface-selective binding process has been explained through potential energy calculations following a simple model. In this Article, the terms complexes and aggregates are being used interchangeably.

2. Materials and Methods

Gelatin B (Bloom no. 75, molecular weight = 90 ± 10 kDa[17]) was supplied by Sigma Chemicals (U.S.), and agar (*Gracilaria dura*, molecular weight ≈ 300 kDa[20]) was generously supplied by CSMRI, Bhavnagar (India), and other chemicals used were of analytical grade bought from Merck. The polydispersity index for both was not known. However, agar powder contained metal ions at ppm level.[20] For gelatin, Sigma Chemicals does not provide this information. The titration data of carboxylic groups on agar were not available. The solvent used was deionized water. Typically, 0.1% (w/v) gelatin solution was prepared by dissolving gelatin powder in the solvent at 40 °C and mixing it for 1 h using a magnetic stirrer. Agar solution (0.1% w/v) was prepared by autoclaving. Equal volumes of both solutions were mixed at room temperature (20 °C), and the ionic strength of the mixture solutions was set to 0, 0.01, 0.05, and 0.1 M using NaCl which generated four interacting solutions. Following identical procedure, three sets of each of the solutions were made. Each sample was stirred for about 1 h for homogeneous mixing. In a typical experiment, the pH of the sample was raised to around 10 using 0.1 N NaOH, and the pH was slowly reduced by titrating the sample with 0.1 N HCl. The extent of intermolecular interactions could be easily monitored through quantitative measurement of solution turbidity. The change in transmittance (%T) of the solution was monitored continuously using a turbidity meter (Brinkmann-910, Brinkmann Instruments, U.S.) operating at 450 nm. This was continued until a maximum turbidity was registered. The turbid samples were sealed and stored at room temperature (20 °C) for ∼3 days (to increase the yield) and then subjected to centrifugation at 10 000 rpm for 30 min, which separated the turbid solution into two distinct liquid phases, the dense coacervates at the bottom and supernatant at the top. The polymer-rich phase at the bottom was collected after decanting the supernatant. This was repeated at least three times, which yielded the coacervates. This is the normal procedure of extracting the coacervate from the reacted solutions.[21−24] These coacervate samples were analyzed by rheology and SANS to probe their viscoelastic and microstructural properties.

The zeta-potential measurements were performed on an electrophoresis instrument (model: ZC-2000, Microtec, Japan). The individual biopolymer and coacervating solutions were diluted 10 times to know the surface charge of streaming particles. In case of the interacting solutions, if one uses the zeta potential (Z) as an approximation of the surface potential φ of a uniformly charged sphere, the theory gives[25]

$$Z \cong \varphi = 4\pi(\sigma/\varepsilon\kappa) \quad (1)$$

where σ is the surface charge density of the particle, and ε and κ are the dielectric constant and Debye−Hückel parameter of the solution, respectively. It has been shown that to a very good approximation the surface potential can be determined from the potential existing at the hydrodynamic slip plane, which is called the zeta potential. The relationship between the mobility (μ) and the zeta potential is $Z = 4\pi(\mu\eta/\varepsilon)$. Next, μ can be written as $\mu = \sigma/\eta\kappa$ where η is the viscosity of the solution. Because the polyelectrolytes are in random coil conformations, the quantitative application of eq 1 is not expected.

Rheological measurements, using small amplitude oscillatory shear, were performed on the agar−gelatin coacervates using controlled stress AR 500 rheometer (TA Instruments, Surrey, England). For all of the tests, the storage modulus (G') data were computed from raw dynamic oscillatory data using TA Instrument Rheology Advantage Data Analysis software (version 3.0.1). All measurements were performed in triplicate to ensure data reproducibility (relative standard deviation less 5%) for each sample. The rheological studies were carried out in two independent sets of experiments that comprised temperature and frequency sweep measurements.

The melting temperature of the coacervate samples was probed by performing isochronal temperature sweep experiments using cone−plate geometry (2 cm diameter, 2° cone angle, and 56 mm truncation gap). The samples were loaded onto the peltier plate (20 °C) of the rheometer and allowed to equilibrate for 10 min. The periphery of the geometry was coated with light silicon oil and enclosed within a wet sponge supplied by the manufacturer to minimize solvent evaporation. Temperature dependence of dynamic storage modulus was recorded by heating the sample from 20 to 95 °C. The angular frequency was fixed at 6.2830 Hz, and controlled stress was 4.7750 Pa. The melting temperatures (T_m) were determined from the abrupt change in slope of the heating cycle data. In the frequency sweep experiments, coacervate samples of different salt concentrations were loaded onto the rheometer plate preheated to different temperatures ranging from 20 to 40 °C. Measurements were carried out with a cone plate geometry using a constant oscillation stress of 6.3660 Pa. The effect of oscillatory frequency on the dynamic rheological properties of the coacervate network was evaluated at these temperatures after the samples were allowed to equilibrate for 10 min. The mechanical

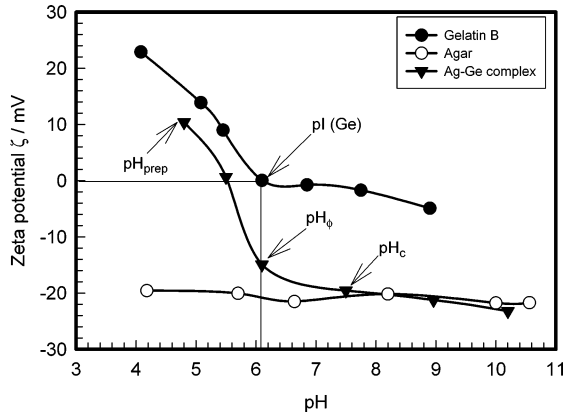

Figure 1. Zeta potential versus pH plot for 0.1% (w/v) gelatin B, 0.1% (w/v) agar, and Ag−Ge complexes (diluted 10 times). Note the pI of gelatin B is at pH = 6.

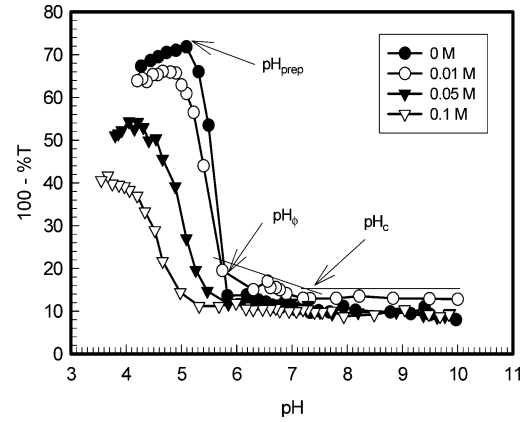

Figure 2. Titration profile of interacting solutions of the two biopolymers recorded at 20 °C. The titration was performed from pH = 10 toward lower pH values. The change in turbidity was observed at pH_c, pH_Φ, and pH_{prep}. The first appearance of turbidity seen at pH_c is indicated as a change in the slope of turbidity versus pH curve.

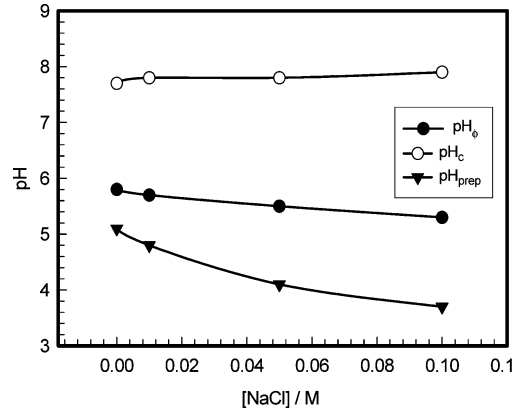

Figure 3. The plot shows the variation of pH_c, pH_Φ, and pH_{prep} as a function of NaCl concentration. Note that pH_c and pH_Φ are invariant of NaCl concentration, while pH_{prep} shows a decreasing trend with increase in NaCl concentration. Solid lines are to guide the eye.

spectra were characterized by observing (G') as a function of angular frequency (ω) in the range of 0.628−100 rad/s.

The static structure factor of coacervate samples was measured by small angle neutron scattering experiments performed at the Dhruva reactor, Bhabha Atomic Research Centre, Mumbai, India. The wavelength of the neutrons used covered the scattering vector (q) range $1.8 \times 10^{-2} \leq q \leq 3.4 \times 10^{-1}$ (Å)$^{-1}$, given by $q = (4\pi/\lambda) \sin \theta/2$, λ being the wavelength of neutron and θ the scattering angle. The dense polymer phase coacervate was transferred to a quartz cell, and the scattered intensity was measured as a function of scattering vector. The measured intensity was corrected for the background, and the empty cell contribution and the data were normalized to get the structure factors.

3. Results and Discussion

The phenomenology of formation of intermolecular complexes leading to phase separation depends on the physical environment of the system. Thus, the pH, polymer charge density, ionic strength, temperature, and mixing ratio, all play a vital role in the formation of the complexes. The intermolecular complex formation is an associative interaction involving the attractive forces and entropy of the system. Thus, it is imperative to begin such studies with the electrophoretic characterization of the samples.

3.1. Electrophoretic Studies. The electrophoretic behavior of agar and gelatin molecules as well as their intermolecular complexes was studied at room temperature. To understand the mechanism of formation of the Ag−Ge complex, the zeta potentials of 0.01% (w/v) agar and 0.01% (w/v) gelatin B solutions were measured separately at different pH. Measurement on agar−gelatin intermolecular complexes at different pH was also carried out after dilution of the samples by 10 times. Because the net surface charge of the system is not much affected by its dilution, the data can be assumed to be comparable to the original system. No reliable measurements could be performed on samples prepared with salt. The representative data are shown in Figure 1. The results reveal that the pI of gelatin was close to 6 and agar was a polyanionic molecule with zeta potential ≈ −20 mV. Beyond pH = 6, gelatin molecules were weakly charged with a small negative zeta potential ≈ −5 mV. The titration profile shown in Figure 2 implies that first appearance of turbidity was noticed at pH_C = 7.4. This refers to the formation of intermolecular soluble aggregates. Thus, the two polyions could form aggregates when the net charge on both was negative. The turbidity continued to rise, and a peak was observed at $pH_\Phi \approx 6$, and even at this pH, both biopolymers continued to carry similar charge. The soluble aggregates precipitated out of the interacting solution at $pH_{prep} \approx 4.5$. This is the point of maximum interaction and a stage for rapid formation of coacervates.

3.2. Turbidimetric Titration. Turbidity measurements were performed on gelatin B−agar solutions prepared with mixing ratio = 1:1 and NaCl concentrations of 0, 0.01, 0.05, and 0.1 M at various pH's ranging from 10 to 4 (Figure 2). Figure 3 shows clearly how various transition pH's vary with NaCl concentration. At pH_c (= 7.4, Figure 2), there is slight turbidity showing the initiation of intermolecular binding between gelatin and agar chains forming soluble aggregates. Here, both agar and gelatin molecules are negatively charged, because pH_c > pI of gelatin B (pI ≈ 6) (Figure 1). Yet gelatin, being a polyampholyte, still has some positively charged patches on its surface to promote surface-selective binding at these locations. One could observe no change in pH_c with change in NaCl concentration (Figure 3), suggesting no significant role played by the mobile ions in screening the interactions and affecting the binding. At pH_Φ (near pI of gelatin), the gelatin molecules have a minor net positive charge on its surface, and hence the coacervation process is enhanced showing rapid charge neutralization and significant increase in turbidity. With further lowering of pH, a similar trend was observed until the soluble aggregates precipitated out at pH_{prep} (= 5 ± 0.2, see Figures 1

and 2). Salt screening effect is clearly not seen from the data presented in Figure 3, where pH_C and pH_Φ values remained invariant of the ionic strength, which is a characteristic signature of surface patch binding phenomenon. This indicated that the intermolecular interactions were poorly screened by mobile ions. The ability of the system to undergo coacervation transition in the absence of salt implies that the two biomolecules followed a symmetric binding character as far as the stoichiometry was concerned. There was a notable change in pH_{prep} from pH 5 to 4.2, which was observed on increasing salt concentration. This depicts that the mobile ions stabilize the system on pH change.

Normally, for $pH > pH_\Phi$, one observes the formation of large insoluble complexes that undergo precipitation immediately, which is observed in the turbidity−pH profile data as a sharp drop in measured turbidity values.[21,22] In the present case, it was observed that for $pH > pH_\Phi$ the turbid solution did not undergo precipitation instantaneously, and we found a flat or saturated type of curve (Figure 2) extending beyond the maximum turbidity pH, but the precipitation occurred within 15 min. This can be explained in the following way. Initially, the size of the insoluble aggregates was small, which was not conducive for instantaneous precipitation. These aggregates grew to a larger size with time following Ostwald ripening, and eventually precipitation ensued. These insoluble aggregates were not amenable to electrophoresis measurements because these dispersions sedimented gradually. At pH_Φ, a binding saturation was reached that was dictated by the stoichiometry of the polymers involved.

3.3. Surface-Selective Patch Binding. Agar is a polyanionic bioploymer that exhibits strong polyelectrolytic character in the entire range of pH. The pI of gelatin is 6, which means when $pH < pI$, it behaves as a polycationic molecule, and when $pH > pI$, it shows polyanionic characteristics. The intermolecular binding for all four samples was initiated near $pH_C = 7.2$ as observed from the turbidity experiments (Figure 2). However, we also observed a significant increase in turbidity at $pH_c < pH < pH_\Phi$. In this range, the gelatin molecule acquires small positive charge on its surface, although the overall charge still remains negative.[24] Again, when we consider the stiffness of the polymer chains, agar, having all negative charges on it, is stiffer than the gelatin molecule, which has both positive and negative charges over it. The agar molecule cleverly selects those patches on the gelatin molecule that are positively charged and binds to it selectively to yield intermolecular complexes. This mechanism is well-known as surface-selective patch binding and is elaborately explained earlier.[15,23] This mechanism is also supported by the electrophoretic data given in Figure 1. Zeta potential data of complexes indicate that there is an intermolecular charge neutralization mechanism involved that resulted in producing these complexes bearing intermediate charge.

A simple model calculation has been performed to show the importance of electrostatic potential energy in surface-selective binding mechanisms. The electrostatic charges on the agar and gelatin particles are determined separately from the Smoluchowski approximation using zeta potential data[25]

$$Q = (3/2)\cdot\varepsilon\cdot R_h\cdot Z \quad (2)$$

where ε is the permeability of the medium, R_h is the hydrodynamic radius of the particle, and Z is the zeta potential of the particle. A representative estimation of electrostatic interaction energy can be carried out in the pH window 4−9 where most of the kinetics is located. The apparent hydrodynamic radius R_h of gelatin is 50 nm,[17] and that of agar is 100 nm (measured).

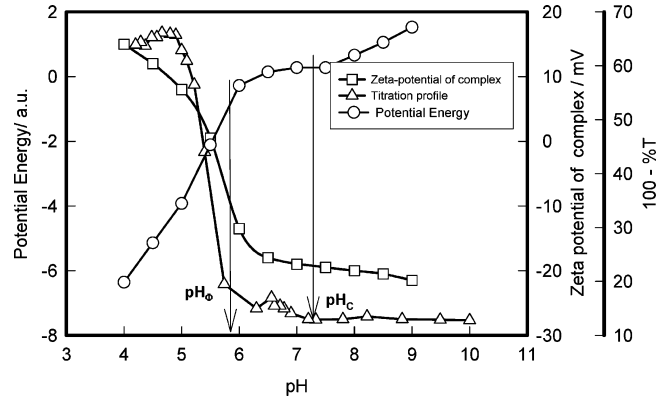

Figure 4. Electrostatic potential energy (in arbitrary units) between agar and gelatin molecules at intermolecular distance $d_s = 55$ nm. The zeta-potential plot of agar−gelatin intermolecular complexes and a titration plot are included for qualitative comparison of transition pH's. Notice that at pH_C and pH_Φ the potential energy undergoes abrupt change. Solid lines are to guide the eye.

The intermolecular distance can be determined from concentration and molecular weight as

$$\text{number density of agar in the solution } N_{Ag} = (N_A/100)\cdot C_{Ag}/M_{Ag} \quad (3)$$

$$\text{number density of gelatin in the solution } N_{Ge} = (N_A/100)\cdot C_{Ge}/M_{Ge} \quad (4)$$

where C_{Ag} and C_{Ge} are the concentrations of agar and gelatin in the system, M_{Ag} and M_{Ge} are the molecular masses of agar and gelatin molecules, respectively, and N_A is Avogadro's number.

$$\text{intermolecular distance in the system } d_s = (1/(N_{Ag} + N_{Ge}))^{1/3} \quad (5)$$

The intermolecular distance d_s was estimated to be ~63 nm in this particular system. Gelatin is a polyampholyte bearing 13% of residues that are acidic and 15% residues are basic in nature (Merck Index data). Assuming that all of the acidic residues are deprotonated and all basic residues are protonated at $pH_C \approx 7$, the chain has a surplus of 2% positively charged patches that electrostatically bind to agar molecule. Because the intermolecular separation and charge on agar and gelatin are known, it is possible to estimate the potential energy of interaction between the two biopolymers given by

$$\text{potential energy} \approx (1/4\pi\varepsilon)(Q_{Ge}Q_{Ag}/d_s) \quad (6)$$

where the excess charge on gelatin is Q_{Ge} and charge on agar molecule is Q_{Ag}. The potential energy is plotted as function of pH in Figure 4, and for convenience it is plotted in arbitrary units for comparison with titration profile data. The zeta potential of intermolecular complexes is also plotted in the same graph. The potential energy plot is quite revealing. There is strong attraction between the agar and gelatin chains as one goes for $pH < 6$. The pH_C is clearly discernible in the plot where potential energy shows reduction and intermolecular complexes have a zeta potential ≈ −20 mV. At the maximum turbidity point

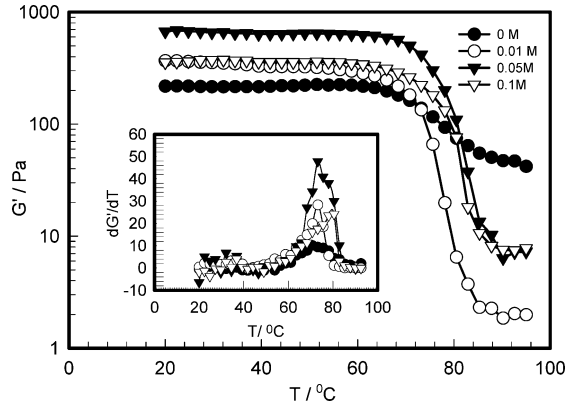

Figure 5. Plot of storage modulus, G', as a function of temperature for coacervate samples. A sharp drop in G' value indicates a melting transition. The temperature derivative of G' is shown in the inset where peaks indicate melting temperature. Solid lines are to guide the eye.

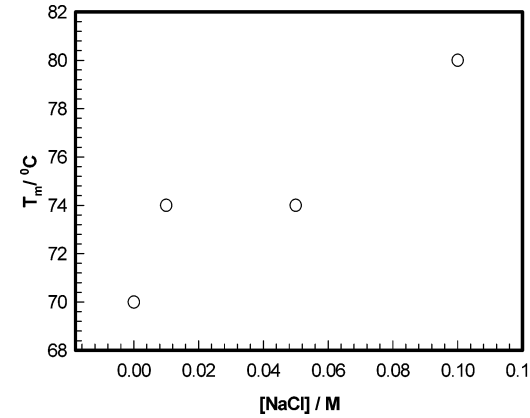

Figure 6. Plot of melting temperature of coacervate samples as a function of salt concentration. Notice that melting temperature increases with increasing salt concentration.

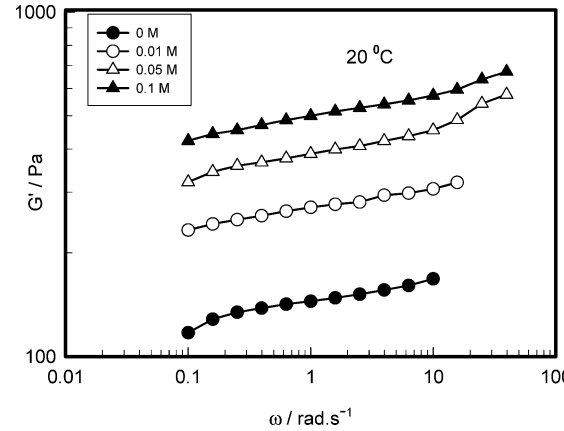

Figure 7. Frequency sweep plots of coacervate sample at various salt concentrations taken at temperature of 20 °C. These data fit very well to the power-law function (solid lines). See text for details.

(pH_Φ), a sharp drop in potential energy is noticed that corresponds to strong intermolecular binding maximum and rapid coacervation. The mid point between pH_Φ and pH_{prep} is located at pH ≈ 5.4 where the intermolecular complexes achieve complete charge neutralization (zero zeta potential). At this pH, the potential energy changes its slope again, allowing coacervation to proceed aggressively. For pH > 7.5, there is strong intermolecular repulsion, which can be noticed as a sharp rise in the potential energy curve. Complex formation and coacervation were observed in the pH range where the two biopolymers had the same type of net charge, which indicates anomalous binding behavior between the two biopolymers, which is the window between the two vertical arrows shown in Figure 4. Maximum yield of coacervate is obtained if these are collected near pH ≈ 5.4. The simple potential energy plot captures all of the salient features of the surface-selective patch binding mechanism prevailing in the present system.

3.4. Characterization of Coacervates. After probing the intermolecular interactions responsible for coacervation transition in this system, it was felt imperative to undertake a thorough thermo-mechanical characterization of the polymer-rich phase of the reacted solutions (coacervates). While the viscoelastic properties including the melting behavior were studied by rheology, the internal microstructure was examined through SANS experiments.

a. Melting Temperature. Temperature sweep studies were performed on the extracted coacervate material where the temperature dependence of storage modulus was measured at a fixed frequency (6.2830 Hz), and the data are depicted in Figure 5. The melting temperature corresponds to the abrupt fall in the storage modulus value, which is best noticed if the first derivative of G' (dG'/dT) is plotted against the temperature (inset of Figure 5). The melting temperature for the system was around 75 °C, which was different from the gels of its constituents. No melting was observed around 30 or 85 °C, which correspond to gelatin and agar gel melting temperatures.[26,27] Thus, the coacervate material was a new biomaterial bearing no physicochemical resemblance to its constituent biopolymers. The effect of screening of interactions due to the presence of mobile ions can have bearing on the melting temperature, which is clearly seen from the data shown in Figure 6. The melting temperature is observed to increase with ionic strength by as much as 10 °C. This may be due to the formation of salt-bridges in the system that increases the mechanical rigidity of the material. On comparing these results with agar gels, one can also argue that such behavior owes its origin to the presence of gel-like (physical) network structures inside the coacervate phase.

b. Viscoelastic Properties. Figure 7 shows the frequency sweep studies performed on the various coacervate samples at 20 °C. The data indicate that although the dispersion behavior was qualitatively similar the samples with higher ionic strength were associated with higher storage modulii, again implying that the mobile ions established salt-bridges between the biopolymers to enhance the mechanical rigidity of the material. Figure 8 shows the frequency sweep curves at different temperatures (20−35 °C) for no salt sample. Other samples showed similar frequency dependence. The linear viscoelasticity model, for pre- and postgel situations, proposed by Winter[28] predicts that the stress-relaxation in the material allows the storage modulus to follow the power-law frequency dependence behavior given by

$$G' = S\omega^n \text{ with } 0 < n < 1 \tag{7}$$

where S is the elastic strength of the material and n is the exponent indicative of the nature of cross-linking. If $n < 0.5$, it shows an excess of cross-linker, and when $n > 0.5$ there is a lack of cross-linker. However, this formalism is strictly applicable to chemically cross-linked gels, and strictly speaking our system is different from that of the system of gels. In the present samples, the cross-linking is provided by surface patch

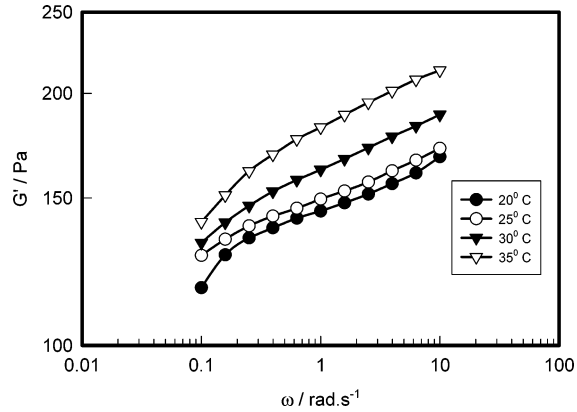

Figure 8. Frequency sweep plots at various temperatures 20, 25, 30, and 35 °C are shown for a salt-free coacervate material. Solid lines are power-law fitting to the data that yield the power-law exponent n and rigidity strength of the material, S.

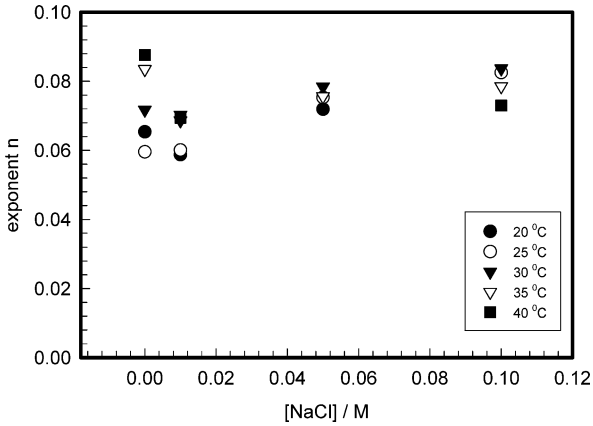

Figure 9. Variation of exponents n as a function of salt concentration at various temperatures. The exponent is less than 0.1 for almost all cases, showing weak cross-linking in the system. See text for details.

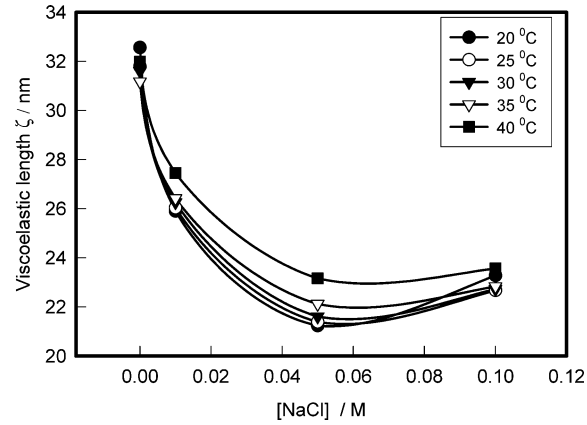

Figure 10. Plot of viscoelastic length of coacervate samples as a function of salt concentration at various temperatures. Notice that samples with higher salt concentration were associated with shorter viscoelastic lengths.

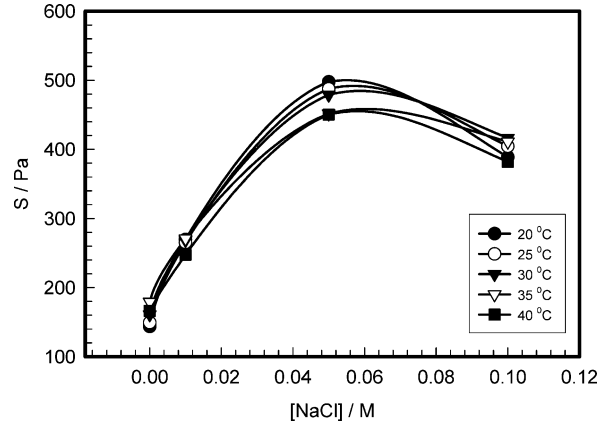

Figure 11. Plot of mechanical rigidity strength of coacervate samples as a function of salt concentration at various temperatures. Samples with higher salt concentration produced stronger coacervate materials.

binding. The G' values could be measured in a very narrow frequency range, 0.1−20 rad/s, with reliability. This value remained close to few hundred Pa for all of the samples. The G'' data were extremely noisy and unrealistically small. The plateau region in G' is normally observed for strongly cross-linked chemical gels. In case of physical gels, such a region is often not seen. We have treated the coacervate materials as a poorly cross-linked gels due to the fact that these yielded measurable G' values that were consistently larger than G'' data. The data shown in Figure 8 were fitted to eq 7 that yielded the exponent n. This exponent was determined to be ∼0.1, implying the existence of a weakly cross-linked system (Figure 9). The coacervate system is highly rich in polymers as compared to gels and lacks in free solvent diffusion process within the network.

Pierce and Carey[29] studied the flow of fluids in a host medium containing obstacles. Following their model, it can be argued that the no-slip condition at the interfaces tends to force the water to move with the network, but the finite viscosity allows the water at small distances from the interfaces to move at a different velocity than the networks. The apparent driving force for the interstitial water relative to the networks is associated with the inertia of the water and is proportional to the difference in densities, which attributes a different viscosity to interstitial as compared to bulk water. Coacervates trap some amount of interstitial water molecules whose viscosity can be conceived to be much higher than the water trapped inside the gel network. The Winter model[28] is applied to the rheological data obtained from coacervate samples to have a feeling of the elastic nature of the system. From Figure 9, one can easily ensure that the presence of salt increases the cross-linking inside the system as expected.

The viscoelastic length L was determined (Figure 10) from the relation[30]

$$G_0 = K_B T/L^3 \tag{8}$$

where K_B is the Boltzmann constant, T is the absolute temperature, and G_0 is the elastic storage modulus at low frequency where $\omega = 0.1$ rad/s. The viscoelastic length (typical distance between polymer-rich and polymer-poor regions, the values remained within the window 32−22 nm) for the coacervate samples was found to be almost invariant of temperature, but it was strongly dependent on ionic strength. The viscoelastic length decreased with increased mobile ion concentration, indicating that at higher ionic strength the biopolymers were strongly bridged. Figure 11 depicts the elastic rigidity of the coacervates for different ionic strengths and temperatures. The gel strength was also found to be independent of temperature, but it increased with increase in NaCl concentration. Here too we can see the footprint of salt-bridges that helped to strengthen the coacervate

systems. This clearly shows the role played by mobile ions in stabilizing the internal microstructure of coacervates.

c. SANS Studies. In the SANS studies, the mean field theory reveals that polymers in a good solvent at equilibrium show a structure factor arising from concentration fluctuations in the intermediate-q region, known as the Ornstein−Zernike (O−Z) function, which is given by[31]

$$S_L(q) = S_L(0)/(1 + q^2\xi^2); q\xi \gg 1 \quad (9)$$

where ξ is the correlation length of the fluctuations and it can be associated with the size of the entangled network. Physically $S_L(0)$ is related to the cross-linking density and longitudinal osmotic modulus of the network. If the spatial scale of density fluctuations due to the presence of inhomogeneities is large as compared to the correlation length ξ, then the two contributions can be treated separately, and an additional contribution to structure factor, $S_{ex}(q)$, arises from long length scale concentration fluctuations (small-q). Thus, the total structure factor can be written as[32,33]

$$S(q) = S_L(q) + S_{ex}(q) \quad (10)$$

where $S_L(q)$ is the Ornstein−Zernike (O−Z) function, and the Debye−Buche (D−B) structure factor has $S_{ex}(q)$ as given by[33]

$$S_{ex}(q) = S_{ex}(0)/(1 + q^2\zeta^2)^2 \quad (11)$$

where $S_{ex}(0)$ is the extrapolated structure factor at zero wave vector and ζ is the size of inhomogeneities present in the system. As $S_{ex}(q) \propto 1/q^4$, the D−B contribution dominates over the O−Z function at low-q, whereas at intermediate-q ($S_L(q) \propto 1/q^2$), the O−Z function contributes the most to the scatter. Recall that coacervates are amorphous substances and are devoid of any spatial ordering (coacervation transition is a first-order phase transition). This would imply identical scattering profiles for all of the samples, which will be observed if and only if the intermolecular interactions are so strong that mobile ion-induced Debye−Huckel screening is not too effective. Because $S(q)$ depends on the square of the difference of neutron scattering length densities of the scatterer and the solvent, it cannot distinguish between microscopic structures of two samples with identical concentrations, particularly when both are amorphous materials. A typical SANS plot is shown in Figure 12.

The SANS data, collected at room temperature, were fitted to the O−Z function in the wave vector region $7.2 \times 10^{-2} \le q \le 3.4 \times 10^{-1}$ (Å)$^{-1}$ and to the D−B function in the region $1.8 \times 10^{-2} \le q \le 7.2 \times 10^{-2}$ (Å)$^{-1}$ (Figure 12). This yielded the values for the correlation length and size of inhomogeneities, which is shown in Figure 13 as function of salt concentration of the samples. The correlation length shows no dependence on ionic strength, whereas the size of inhomogeneities increased by close to 50%. Thus, the presence of mobile ions contributed to the increase in heterogeneity inside the coacervate.

Evaluation of small-angle neutron scattering (SANS) data is often complicated by multiple scattering effects if large particles of relatively high volume fraction have to be studied and dilution or contrast reduction is impossible. Multiple scattering corrections in small-angle neutron scattering experiments on such samples have been examined. Numerical calculations show that, for such typical experimental conditions, the second-order scattering is less than 2% of the first-order scattering for qL up to 10.0, where L the length that is being measured.[34] In our system, $L \approx 30$ Å and q_{max} is 0.3 (Å)$^{-1}$, which satisfies the said condition. Thus, it was not necessary to undertake any correction for secondary scattering. Another issue that clouds SANS data concerns observation of correlation peak. The raw SANS data clearly showed the absence of correlation peak at low-q, and scattering profiles for samples, with and without salt, were observed to be identical because no preferential spatial correlation develops in the material due to presence of mobile ions. However, the data yielded different inhomogeniety size and correlation length as the salt concentration was altered. The behavior is typical of polymer gels (and their sols), which has been extensively reviewed by Hashimoto.[35] In fact, Hashimoto has examined a host of soft matter systems, but none showed any correlation peak in the low-q region. Leisner and Imae[36] examined complex coacervation in polyglutamic acid-polyamido amine dendrimers by SAXS and light scattering. Here too no correlation peak was seen.

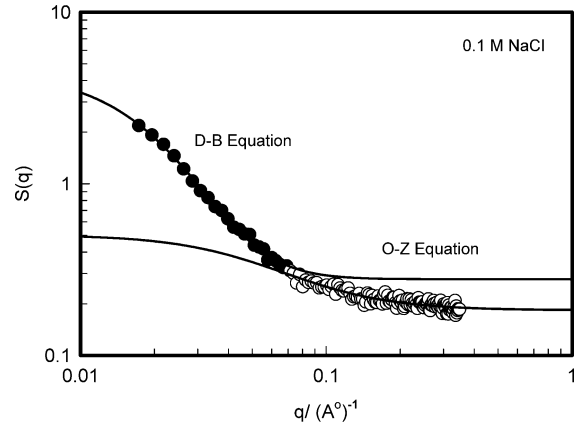

Figure 12. Typical SANS experimental data of the coacervate sample ($I = 0.1$ M NaCl) recorded at 20 °C. Solid line is fitting to D−B and O−Z equations with $\chi^2 > 0.9$. See text for details.

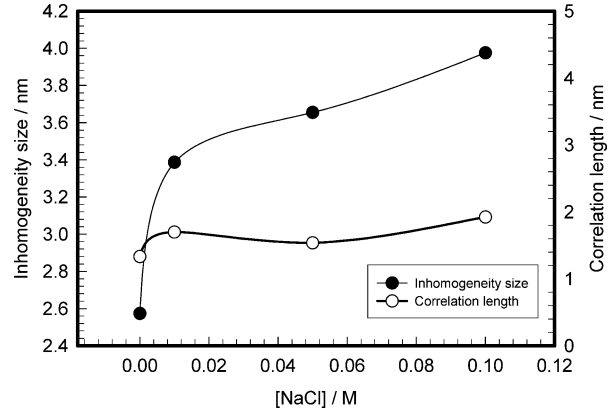

Figure 13. The plot depicts the size of inhomogeneities and characteristic length for various coacervate samples determined from the SANS data shown in Figure 12.

3.5. Comparison with Other Coacervate Systems. A relative comparison of physicomechanical properties of various coacervate systems is given in Table 1. These systems were probed by SANS and rheology experiments performed in our laboratory. Hydrophobic interactions in addition to that of electrostatic and solute−solvent interactions facilitate coacervation transition in gelatin solutions, which has been discussed in details in ref 17. The occurrence of phase separation in the system was attributed to the change in volume fraction of the nonsolvent added to the homogeneous aqueous solution of gelatin. It was reported

TABLE 1: Comparison between Various Coacervates of the Agar and Gelatin System[a]

analysis	[1]gelatin[17]	[2]gelatin A:gelatin B[18]	[2]gelatin A:chitosan[15]	[2]gelatin A:agar[2]	[2]gelatin B:agar (this work)
binding type	electrostatic	electrostatic	surface selective	electrostatic	surface selective
transition pH values	alcohol driven at constant pH	$pH_c \approx 5.5$, $pH_\Phi \approx 6.3$	$pH_c \approx 4.5$, $pH_\Phi \approx 6.5-7.5$	$pH_c \approx 5.4$, $pH_\Phi \approx 9$	$pH_c \approx 7.5$, $pH_\Phi \approx 6$
effect of ionic strength	yes	yes	none	yes	none
optical nature	opaque	opaque	opaque	semitransparent	semitransparent
network structure	$\zeta = 20$ nm, $\xi = 1.2$ nm		$\zeta = 21-26$ nm, $\xi = 1.2$ nm	$\zeta = 22$ nm, $\xi = 1.2$ nm	$\zeta = 3.2$ nm, $\xi = 1.6$ nm
melting temperature	33 °C	42 °C	64, 87 °C	35, 75 °C	75 °C
viscoelastic property	viscous	viscoelastic	viscous	viscous	viscoelastic

[a] Legends: [1]simple coacervate, [2]complex coacervate, inhomogeneity length = ζ, correlation length = ξ, onset of turbidity at pH_c, turbidity maximum at pH_Φ.

that salt had promoted the coacervation process.[17] In the gelatin A−gelatin B complex coacervate system,[18] there was purely electrostatic interaction induced by pH change, which led to the liquid−liquid phase separation. However, the salt dependence was not reported. In case of gelatin−chitosan complex coacervation, the intermolecular association was initiated by surface-selective patch binding followed by charge neutralization process.[15] The presence of salt had hardly any significant effect over the binding of the two biopolymers. The same type of qualitative behavior was observed in the present case, and we noticed hardly any evidence of ionic strength in the binding process although the same affected the thermo-mechanical properties of coacervates considerably. The SANS data profile of different coacervate samples inferred similar static structure factors; however, there was a variation in length scales in different systems. Our system had less heterogeneity and larger characteristic size as compared to that of the gelatin simple coacervate and its other complex coacervates discussed above. There were no reports for SANS study of gelatin A−gelatin B complex coacervates.

The melting temperature for the gelatin simple coacervate (33 °C) was near the melting temperature of gelatin gel.[26] However, there was a significant shift to 42 °C in case of gelatin−gelatin complex coacervate,[18] which was due to the change in type of binding. In the gel system, network formation is due to hydrogen bonding, and in case of coacervates, it is due to electrostatic binding. The complex coacervate of gelatin is bonded more strongly than that of the simple coacervates. In the gelatin−chitosan complex coacervate, there were two melting temperatures.[15] One of these was close to the agar gel melting temperature[27] (∼85 °C). In gelatin A−agar complex coacervate, there were also two melting temperatures, one being near to the melting temperature of gelatin gel[19] and the other at 75 °C. However, in our present system, we recovered only one melting temperature near 75 °C, which was different from the melting temperatures of its constituent polymer gels.[26,27] Hence, one can see some signature of gelatin gel in the gelatin A−agar complex coacervate system, but no signature of the same in gelatin B−agar complex coacervate. This indicates that there must be a differential binding mechanism and charge neutralization process between the agar and gelatin B and agar−gelatin A samples. It is concluded that the former is governed by surface-selective patch binding, while the latter is due to pure Coulombic interactions.

The rheology studies on the gelatin simple coacervates,[17] gelatin−chitosan complex coacervate,[15] and gelatin A−agar complex coacervate[19] reported in literature reveal that they are viscous in nature, while the gelatin A−gelatin B complex coacervate[18] and gelatin B−agar complex coacervate are viscoelastic in nature. The correlation lengths measured in gelatin simple coacervates were the same as those recorded in gelatin−chitosan and gelatin A−agar complex coacervates (∼1.2 nm), while the size of inhomogeneities ranged between 20 and 26 nm. The present system exhibits correlation length = 1.6 nm and size of inhomogeneities = 3.2 nm. This clearly differentiates the microstructural properties exhibited by various coacervate samples, which, in turn, is governed by the specificity of the intermolecular binding mechanism. The structure and phase ordering kinetics in the coacervation of β-lactoglobulin and acacia gum were investigated in detail by Sanchez et al.[37,38] Multiple growth processes during phase separation were observed in this system that was compatible both with late stage spinodal decomposition and with nucleation and growth descriptions. In a related study,[39] Sanchez and Renard showed that protein aggregates governed the complex coacervation between β-lactoglobulin and acacia gum molecules, both by entropic and by enthalpic effects. The results revealed that composite dispersions containing both protein aggregates embedded inside the complex coacervate, and aggregate-free coacervates are formed simultaneously. The charge neutralization mechanism was clearly differentiated in their study. It was clearly shown that the intermolecular complexation between β-lactoglobulin and acacia gum was mainly decided by neutralization of negative charges on acacia gum by positive charges of β-lactoglobulin. In contrast, during coacervation, the charge neutralization of complexes was achieved through lowering of acacia gum negative charges.[37] Weinbreck et al.[40−43] have studied the complex coacervation phenomenon in whey protein and gum arabic solutions and examined the composition and structure of the coacervate phase. The rheological studies revealed the viscous nature of their complex coacervate where G'' dominated over G'. The viscosity of the coacervate was observed to increase with electrostatic interaction between the two biopolymers. The intermolecular complexes were visualized as gum arabic chains cross-linked by electrostatic interactions with whey protein molecules.[43] Thus, it appears that for each coacervation process there exists signature interaction, rheological behavior, and phase stability roadmap although some broad observables are common to all.

4. Conclusion

Agar, a polyanionic polysaccharide, was shown to undergo liquid−liquid phase separation in the presence of a polyampholyte, gelatin B, even though both biopolymers had similar net charge. The interesting part was that it had no noticeable dependence on the ionic strength of the samples as far as the binding process was concerned. The titration and zeta-potential profile data supported this observation. The coacervation process started with the surface-selective patch binding when both molecules, agar and gelatin, had a majority of negative charge on them, followed by partial charge neutralization and aggregation of coacervate droplets. Because the agar molecule is stiffer than the gelatin molecule, the surface-selective area (positive charge patch) of gelatin molecule binds over the agar rigid rod, and partial charge neutralization takes place. On reaching the

pI of gelatin, the gelatin molecule acquires more positive charge for the charge neutralization to proceed more aggressively. It was found that the salt-bridges helped in stabilizing the internal structure of coacervates. The charge neutralization gets initiated at pH_C and reached its maximum at pH_{prep}. Beyond this pH value, the potential gets contribution from the partially charge neutralized complexes and positively charged gelatin molecules. Regardless, the presence of salt ions was necessary to compensate for charge imbalance present in the soluble complexes and achieve charge neutralization.

The microscopic structure can be imagined as flexible gelatin chain binds to the stiff chain of agar at specific locations and the surface charge is influenced by the surrounding gelatin molecules. Yet the change in the thermo-mechanical properties must be attributed to the presence of both the gelatin and the agar molecules present inside the coacervate material. However, it will be appropriate to argue that the microscopic structure of the coacervate material was comprised of weakly cross-linked polymer-rich zones separated by polymer-poor regions having characteristic viscoelastic length. Such systems are associated with two characteristic relaxation processes: one due to concentration fluctuation and another arising from viscoelastic relaxation. In summary, it has been unambiguously shown that surface-selective binding promotes coacervation transition in the present system of biopolymers, although the electrostatic interactions are not screened by the presence of mobile ions. However, these ions create salt-bridges between the two biopolymers that enhance the thermo-mechanical characteristics of the complex coacervates formed. Surface-selective binding is a poorly understood physical phenomenon, and the present work intends to improve this understanding.

Acknowledgment. S.B. acknowledges the Council of Scientific and Industrial Research, India for a Senior Research Fellowship. We are thankful to Dr. V. K. Aswal for assistance with SANS measurements.

References and Notes

(1) Turgeon, S. L.; Schmitt, C.; Sanchez, C. *Curr. Opin. Colloid Interface Sci.* **2007**, *12*, 166–178.
(2) Singh, S. S.; Siddhanta, A. K.; Meena, R.; Prasad, K.; Bandyopadhyay, S.; Bohidar, H. B. *Int. J. Biol. Macromol.* **2007**, *41*, 185–192.
(3) Boral, S.; Bohidar, H. B. *Polymer* **2009**, *50*, 5585–5588.
(4) Gupta, A. N.; Mohanty, B.; Bohidar, H. B. *Biomacromolecules* **2005**, *6*, 1623–1627.
(5) Pawar, N.; Bohidar, H. B. *J. Polym. Sci., Part B: Polym. Phys.* **2010**, *48*, 555–565.
(6) Jamieson, A. M.; Simic-Glaveski, B.; Tansey, K.; Walton, A. G. *Faraday Discuss. Chem. Soc.* **1976**, *61*, 194–204.
(7) Bungenberg de Jong, H. G. In *Colloid Science*; Kruyt, H. R., Ed.; Elsevier: New York, 1949; Vol. II, Chapter 3.
(8) Sanchez, C.; Renard, D. *Int. J. Pharm.* **2002**, *242*, 319–324.
(9) Overbeek, J. T. G.; Voorn, M. J. *J. Cell. Comp. Physiol.* **1957**, *49*, 7–26.
(10) Veis, A. *J. Phys. Chem.* **1961**, *65*, 1798–1803. Veis, A.; Aranyi, C. *J. Phys. Chem.* **1960**, *64*, 1203–1210.
(11) Nakajima, A.; Sato, H. *Biopolymers* **1972**, *11*, 1345–1355.
(12) Tainaka, K. *Biopolymers* **1980**, *19*, 1289–1298.
(13) Gupta, A. N.; Bohidar, H. B. *Phys. Rev. E* **2005**, *72*, 011507.
(14) Bohidar, H. B.; Dubin, P. L.; Majhi, P.; Tribet, C.; Jaeger, W. *Biomacromolecules* **2005**, *6*, 1573–1585.
(15) Gupta, A. N.; Aswal, V. K.; Bohidar, H. B. *J. Phys. Chem. B* **2007**, *111*, 10137–10145.
(16) Park, J. M.; Muhoberac, B. B.; Dubin, P. L.; Xia, J. *Macromolecules* **1992**, *25*, 290–295. Gao, J.; Dubin, P. L.; Muhoberac, B. B. *J. Phys. Chem. B* **1998**, *102*, 5529–5535.
(17) Mohanty, B.; Bohidar, H. B. *Biomacrolecules* **2003**, *4*, 1080–1086. Mohanty, B.; Bohidar, H. B. *Phys. Rev. E* **2004**, *69*, 021902.
(18) Tiwari, A.; Bindal, S.; Bohidar, H. B. *Biomacromolecules* **2009**, *10*, 184–189.
(19) Singh, S. S.; Aswal, V. K.; Bohidar, H. B. *Int. J. Biol. Macromol.* **2007**, *41*, 301–307.
(20) Meena, R.; Siddhanta, A. K.; Prasad, K.; Ramavat, B. K.; Eswaran, K.; Thiruppathi, S.; Ganesan, M.; Mantri, V. A.; Subba Rao, P. V. *Carbohydr. Polym.* **2007**, *69*, 179–188.
(21) Seyrek, E.; Dubin, P. L.; Tribet, C.; Gamble, E. A. *Biomacromolecules* **2003**, *4*, 273–282.
(22) Kaibara, K.; Okazaki, T.; Bohidar, H. B.; Dubin, P. L. *Biomacromolecules* **2000**, *1*, 100–107.
(23) Dubin, P. L.; Gao, J.; Mattison, K. *Sep. Purif. Methods* **1994**, *23*, 1–16.
(24) Mohanty, B.; Gupta, A.; Bohidar, H. B.; Bandyopadhyay, S. *J. Polym. Sci., Part B: Polym. Phys.* **2007**, *45*, 1511–1520.
(25) Ohshima, H. *Adv. Colloid Interface Sci.* **1995**, *62*, 189–235.
(26) Chatterjee, S.; Bohidar, H. B. *Int. J. Biol. Macromol.* **2005**, *35*, 81–88.
(27) Boral, S.; Saxena, A.; Bohidar, H. B. *J. Phys. Chem. B* **2008**, *112*, 3625–3632.
(28) Winter, H. H. *Polym. Eng. Sci.* **1987**, *27*, 1698–1702.
(29) Pierce, A. D.; Carey, W. M. *Proc. Meetings Acoust. (POMA)* **2008**, *5*, 005001–12.
(30) Onuki, A.; Taniguchi, T. *J. Chem. Phys.* **1997**, *106*, 5761–5770.
(31) De Gennes, P. G. *Scaling Concepts in Polymer Physics*, 2nd ed.; Cornell University Press: Ithaca, NY, 1985.
(32) Koberstein, J. T.; Picot, C.; Benoit, H. *Polymer* **1985**, *26*, 673–681.
(33) Debye, P.; Buche, A. M. *J. Appl. Phys.* **1949**, *20*, 518–525.
(34) Goyal, P.; King, J. S.; Summerfield, G. C. *Polymer* **1983**, *24*, 131–134.
(35) Hashimoto, T. *J. Polym. Sci., Part B: Polym. Phys.* **2004**, *42*, 3027–3062.
(36) Leisner, D.; Imae, T. *J. Phys. Chem. B* **2003**, *107*, 8078–8087.
(37) Sanchez, C.; Mekhloufi, G.; Schmitt, C.; Renard, D.; Robert, P.; Lehr, C. M.; Lamprecht, A.; Hardy, J. *Langmuir* **2002**, *18*, 10323–10333.
(38) Mekhloufi, G.; Sanchez, C.; Renard, D.; Guillemin, G.; Hardy, J. *Langmuir* **2005**, *21*, 386–394.
(39) Sanchez, C.; Renard, D. *Int. J. Pharm.* **2002**, *242*, 319–324.
(40) Weinbreck, F.; de Vries, R.; Schrooyen, P.; de Kruif, C. G. *Biomacrolecules* **2003**, *4*, 293–303.
(41) Weinbreck, F.; Nieuwenhuijse, H.; Robijn, G. W.; de Kruif, C. G. *Langmuir* **2003**, *19*, 9404–9410.
(42) Weinbreck, F.; Wientjes, R. H. W.; Nieuwenhuijse, H.; Robijn, G. W.; de Kruif, C. G. *J. Rheol.* **2004**, *48*, 1215–1228.
(43) Weinbreck, F.; Tromp, R. H.; de Kruif, C. G. *Biomacromolecules* **2004**, *5*, 1437–1445.

JP105431T